Journal of the Meteorological Society of Japan, Vol. 80, No. 3, pp. 485–501, 2002

Determination of Regional Land Surface Heat Flux Densities over Heterogeneous Landscape of HEIFE Integrating Satellite Remote Sensing with Field Observations

Yaoming MA

Cold and Arid Regions Environmental and Engineering Research Institute, Chinese Academy of Sciences, Lanzhou, China

Osamu TSUKAMOTO

Faculty Sciences, Okayama University, Okayama, Japan

Hirohiko ISHIKAWA

Disaster Prevention Research Institute, Kyoto University, Uji, Kyoto, Japan

Zhongbo SU, Massimo MENENTI

Alterra Green World Research, Wageningen UR, 6700 AA, Wageningen. The Netherland

Jiemin WANG, and Jun WEN

Cold and Arid Regions Environmental and Engineering Research Institute, Chinese Academy of Sciences, Lanzhou, China

(Manuscript received 14 May 2001, in revised form 27 February 2002)

Abstract

In this study, a parameterization method based on satellite remote sensing and field observations is described and tested for deriving the regional land surface variables, vegetation variables and land surface heat flux densities over heterogeneous landscape. As a case study, the method is applied to the HEIFE area in northwestern China. The regional distribution maps of the NDVI, the MSAVI, vegetation coverage, leaf area index (LAI), surface reflectance, surface temperature, net radiation density, soil heat flux, sensible heat flux and latent heat flux have been determined over the HEIFE area. The derived results have been validated by using the "ground truth". Comparisons between the results derived from the method proposed in this study, and the previous results (in which the land surface variables and surface heat fluxes were directly derived from the Surface Energy Balance Algorithm for Land—SEBAL) have also been given in this paper. The results show that the more reasonable regional distributions of

Corresponding author: Yaoming Ma, Department of Plateau Atmospheric Physics, Cold and Arid Regions Environmental and Engineering Research Institute (CAREERI), Chinese Academy of Sciences (CAS), 260 Dong-gang West Road, Lanzhou, Gansu 730000, China.
E-mail: ymma@ns.lzb.ac.cn

land surface variables (surface reflectance, surface temperature), vegetation variables (the NDVI, the MSAVI, vegetation coverage and the LAI), net radiation, soil heat flux, sensible heat flux and latent heat flux can be obtained by using the method proposed in this study. Further improvement of this method is also discussed.

1. Introduction

The growing concern about climate change, and global environment, has lead to a number of land surface processes studies over heterogeneous areas. As an integrating component of climatic system, land surface process is an important research areas addressed by the WCRP and the IGBP. Most field observation experiments, such as the HAPEX-MOBILHY, the FIFE, the EFEDA, the HAPEX—Sahel, have been carried out in moist or semi-arid regions. Similar research carried out in arid, and desertification-threatened regions is limited. The general objectives of the Heihe Basin Field Experiment (HEIFE) are to investigate the physical processes of air-land exchanges of water, heat and momentum, to test and improve the parameterization scheme of such fluxes in GCM applied in arid and semi-arid regions in mid-latitudes.

The HEIFE observation was based in an inland river basin of northwestern China. The experimental region, about 70×90 km^2, covers complex land surface conditions with mainly a large area of Gobi, sand desert and various scales of oasis dispersed along the river and canals. During the experimental period, five basic micrometeorological stations, five automatic weather stations and four groundwater level stations were set in oasis, sand desert and Gobi areas. Each basic micrometeorological station had a 20 m-high profile tower (the tower in Linze oasis is 40 m high). Air temperature, humidity, wind velocity and wind direction were observed at 6 levels of the tower. Short-wave incoming radiation, reflective radiation, long-wave incoming and long-wave outgoing radiation and net radiation were recorded at surface level. Simultaneously ground surface temperature, soil temperature at 5 depths under the surface, and soil heat fluxes at 2 layers were measured. During the experimental period, meteorological data from three routine weather observation stations were collected. Surface runoff and sub-surface hydrological data from three routine hydrological stations in the experimental area were collected for providing the background information. The experiment has been operated successfully for more than two years, and a large amount of data of surface observations have been collected (see Fig. 1).

Some interesting detailed studies concerning surface water and heat budget at some stations have already been reported (e.g., Wang and Mitsuta 1990; Tsukamoto et al. 1992; Wang and Mitsuta 1992; Hu et al. 1994; Maitani et al. 1995; Mitsuta et al. 1995; Tsukamoto et al. 1995; Sahashi 1995; Tamagawa 1996). However, the investigation on the regional distribution of water and heat is not enough for heterogeneous landscape of the HEIFE area (Hu et al. 1994). Remote sensing from satellites offers the possibility to derive regional distribution of land surface heat flux densities over heterogeneous arid land surface in combination with sparse field experimental stations. Several methods using satellite remote sensing data are applied to estimate the regional distribution of surface heat flux densities over the HEIFE area (Wang et al. 1995; Ma et al. 1999), however, these retrieval methods are still in a developing stage. Improvements on the following aspects are needed: (1) surface reflectance and surface temperature were based on the linear regression relationships, which depends on the ground observation; and, (2) the sensible heat flux density was derived directly using the SEBAL (Surface Energy Balance Algorithm for Land) (Bastiaanssen 1995), assuming the regional distribution of air temperature based on a linear regression relationship between air temperature and land surface temperature, and no considering on excess resistance for heat transportation kB^{-1} (assumption $kB^{-1} = 2.3$).

The objectives of this study are: (1) to propose a new remote sensing parameterization method over heterogeneous land surface; (2) to derive regional land surface variables (surface reflectance and surface temperature) and vegetation variables (the NDVI, the MSAVI and vegeta-

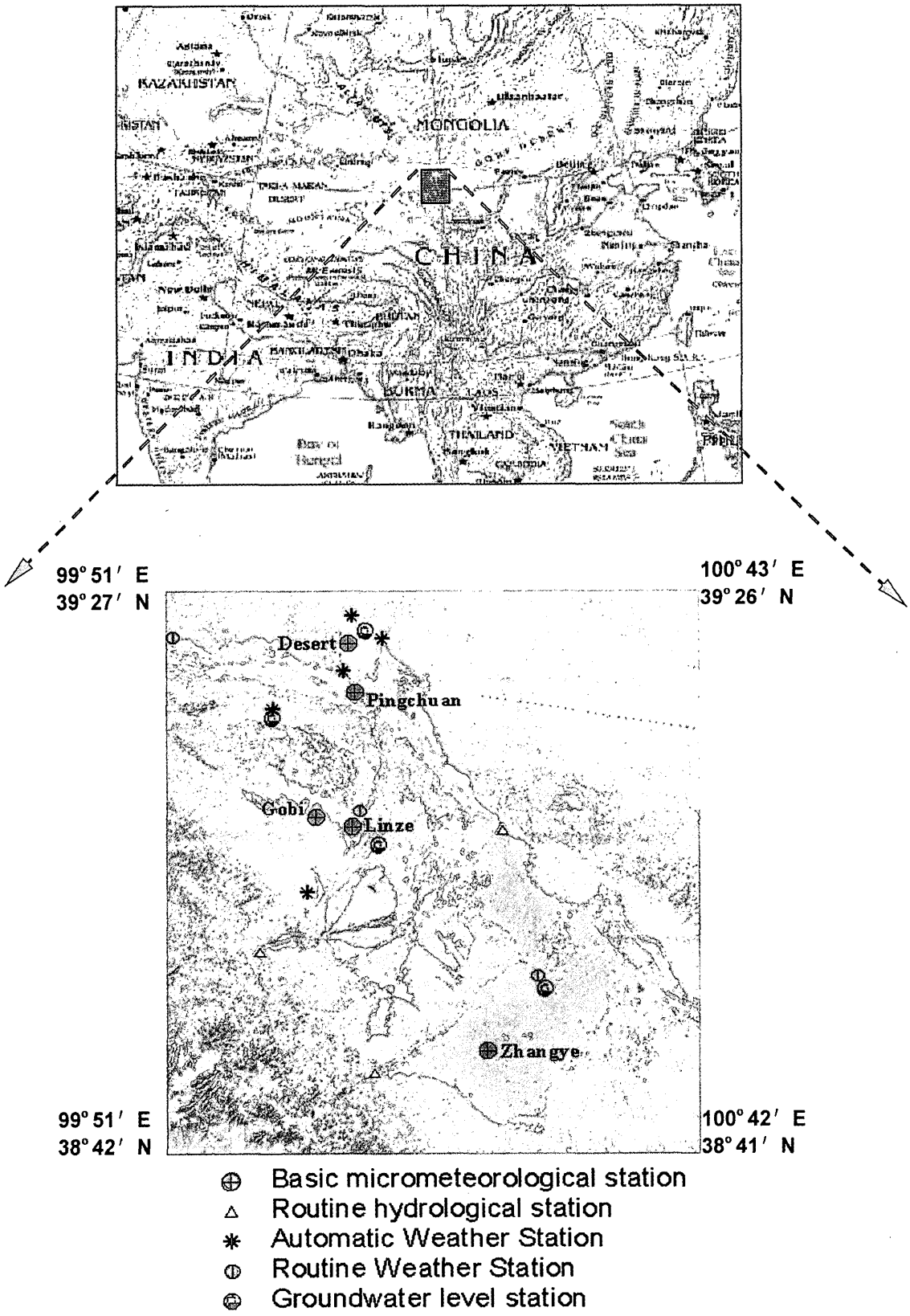

Fig. 1. A composite image of the Landsat TM and the sites layout during IOP of HEIFE, the red part is oasis or irrigated farm, and the others are Gobi desert.

tion coverage) over the HEIFE area with atmospheric correction; (3) to derive the land surface heat flux densities with the new parameterization method over the HEIFE area; and, (4) to compare the derived results with previous studies (Wang et al. 1995; Ma et al. 1999) to validate the new parameterization method.

2. Landsat TM data and field observation data

Landsat Thematic Mapper (TM) provides a spectral radiance in seven narrow bands, with a spatial resolution of about 28.5×28.5 m^2 for three visible bands (Band-1, -2, -3), and three near infrared bands (Band-4, -5, -7), and 120×120 m^2 for the thermal infrared band (Band-6). Because of high spatial resolution of TM, the land surface variables, the vegetation variables and land surface heat flux densities estimated from TM data can be directly compared with the ground measurements (e.g., Wang et al. 1995; Ma et al. 1999; Bastiaanssen 1995). The TM images used in this study was taken at 10:00 (local time) July 7, 1991, over the HEIFE area. This day was very clear when the Landsat TM over-passed the experimental area, and the IOP was just carried out in that day. It means that we have field observational data to calculate the regional surface heat flux, and to validate the derived results from the satellite remote sensing parameterization method.

The most relevant data, collected at the HEIFE surface stations to support the parameterization of land surface heat flux densities and analysis of the TM images, consist of surface radiation budget components, surface radiation temperature, surface reflectance, vertical profiles of air temperature, humidity, wind speed and direction measured at the PBL towers, sodar, radiosonde and tethersonde, turbulent fluxes measured by eddy-correlation technique, soil heat flux, soil temperature profiles, soil moisture profiles, and the vegetation state.

3. Theory and scheme

The general concept of the methodology is shown in a diagram (Fig. 2). The surface reflectance for short-wave radiation (r_0) is retrieved from Landsat TM data with the atmospheric correction by a four-stream radiative transfer assumption for atmospheric correction in solar spectral bands (Verhoef 1997), using aerological observation data. The land surface temperature (T_{sfc}) is also derived from Landsat TM data and aerological observation data. The radiative transfer model MODTRAN (Berk et al. 1989) compute the downward short-wave and long-wave radiation at the surface. With these results the surface net radiation (R_n) is determined. The soil heat flux (G_0) is estimated from R_n, T_{sfc}, r_0, and the MSAVI (Modified Soil Adjusted Vegetation Index, Qi et al. 1994) which is also derived from Landsat TM data. The sensible heat flux (H) is estimated from T_{sfc}, surface and aerological data with the aid of the so called 'blending height' approach (Mason 1988).

3.1 Net radiation

The regional net radiation flux density can be derived from

$$\begin{aligned} R_n(x,y) &= K_\downarrow(x,y) - K_\uparrow(x,y) \\ &\quad + L_\downarrow(x,y) - L_\uparrow(x,y) \\ &= (1 - r_0(x,y)) \cdot K_\downarrow(x,y) \\ &\quad + L_\downarrow(x,y) - \varepsilon_0(x,y)\sigma T_{sfc}^4(x,y), \end{aligned} \quad (1)$$

where $\varepsilon_0(x,y)$ is surface emissivity, K represents the short-wave (0.3–3 μm) and L the long wave (3–100 μm) radiation components, respectively. Surface reflectance $r_0(x,y)$ can be derived from integrated hemispherical planetary reflectance (Koepke et al. 1985; Menenti et al. 1989; Bastiaanssen 1995; Wang et al. 1995; Ma et al. 1999). However, the linear regression relationships are in doubt, because: 1) the ground measurement is only a point value, while the satellite pixel are the average of many point values; 2) fewer ground observation data are coincidence with satellite data relationship (Wen 1999). A four-stream radiative transfer assumption for atmospheric correction in solar spectral bands (Verhoef 1997) is introduced to derive the surface reflectance over the HEIFE area in this study.

The incoming short-wave radiation flux density $K_\downarrow(x,y)$ in Eq. (1), can be derived from radiative transfer model MODTRAN (Kneizys et al. 1996), where atmospheric short-wave transmittance τ_{sw} is obtained. Hence $K_\downarrow(x,y)$

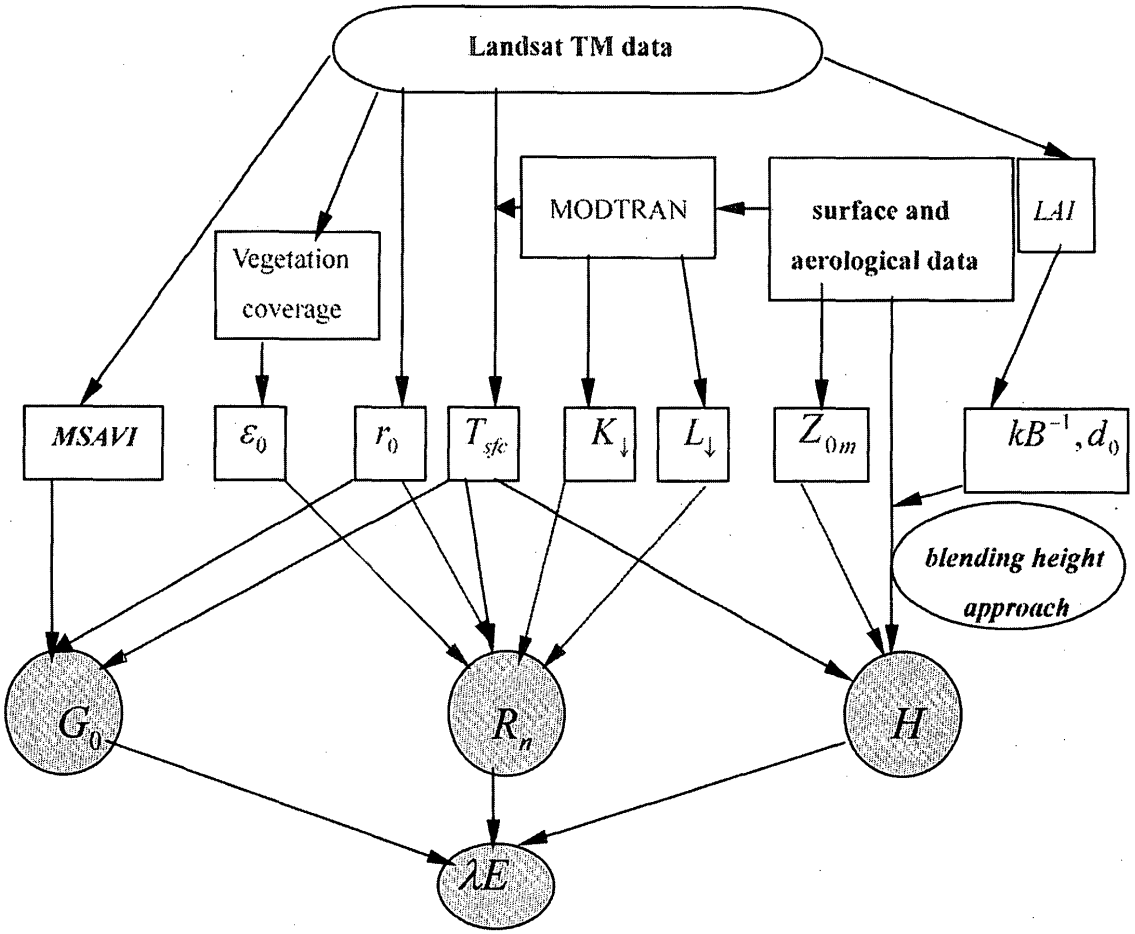

Fig. 2. Diagram of parameterization procedure by combining the Landsat TM data with field observations.

can be obtained as

$$K_\downarrow(x,y) = \tau_{sw} K^\downarrow_{TOA}(x,y), \tag{2}$$

where the regional variation of radiation flux density perpendicular to the top of atmosphere $K^\downarrow_{TOA}(x,y)$ is a spectrally integrated form of in-band radiation flux density perpendicular to the top of atmosphere $K^\downarrow_{TOA}(b)$, and

$$K^\downarrow_{TOA}(x,y) = \frac{K^\downarrow_{exo}(b)\cos\theta_{sun}(x,y)}{d_s^2}, \tag{3}$$

where $K^\downarrow_{exo}(b)$ is the averaged in-band solar exo-atmospheric irradiance undisturbed by θ_{sun} being zero, b is the abbreviation of in-band, d_s is the earth-sun distance, θ_{sun} is sun zenith angle.

The incoming long-wave radiation flux density $L_\downarrow(x,y)$ in Eq. (1), can be derived from MODTRAN directly as well. The surface emissivity of $\varepsilon_0(x,y)$ is a function of the vegetation coverage P_v, it can be derived from the model of Valor and Caselles (1996). Surface temperature $T_{sfc}(x,y)$ in Eq. (1) can be derived from the Landsat TM thermal infrared band-6 (10.2–12.5 μm) spectral radiance. The upward thermal radiance at wavelength λ going through the local atmosphere layer is described by

$$\chi\frac{dL_\lambda}{d\delta} = L_\lambda - B_\lambda, \tag{4}$$

where δ is atmosphere optical thickness, $\chi = \cos\Theta$, Θ is angle between vertical direction and radiative stream, and B_λ is black emitted radiance as given by the Planck function

$$B_\lambda(T) = \varepsilon_0 \frac{2hc^2}{\lambda^5\left[\exp\left(\frac{hc}{k\lambda T}\right) - 1\right]}, \tag{5}$$

where T is absolute temperature, ε_0 is relative emissivity, h is Planck constant, c is light speed, and k is Boltzmann constant. There are following boundary condition for radiative

transfer

$$\begin{cases} L_\lambda(\delta_0,\chi) = B_\lambda(T_{sfc}) & \delta = \delta_0 \\ L_\lambda(0,\chi) = 0 & \delta = 0 \end{cases}, \quad (6)$$

then the upward radiance can be derived after integrating Eq. (4) as

$$L_\lambda(\delta,\chi) = L_\lambda(T_{sfc})e^{(\delta-\delta_0)/\chi} + \int_\delta^{\delta_0} B_\lambda[T(\delta')]e^{(\delta'-\delta)/\chi}\,d\delta, \quad (7)$$

where $L_\lambda(T_{sfc})$ is upward radiance emitted from land surface, δ' atmospheric optical thickness at an arbitrary altitude. The satellite sensor detected radiance $L_S(x,y)$ for each pixel is composed of two elements: contribution from land surface and from atmosphere layer

$$L_S(x,y) = \tau L_0(x,y) + S(x,y), \quad (8)$$

where $L_0(x,y)$ is emitted band radiance from the land surface, $S(x,y)$ is band upward radiance at the top of atmosphere, and τ is band average transmittance. $S(x,y)$, and τ can be derived from the MODTRAN model. Hence, the brightness temperature for each pixel at the land surface $T^B(x,y)$ can be expressed from the Eq. (8) for a given wavelength, or remote sensor band as (Wang et al. 1995)

$$T^B(x,y) = c_2/[\ln(c_1/L_0(x,y) - 1], \quad (9)$$

where c_1 and c_2 are constants. Therefore, the distribution of land surface temperature is obtained as

$$T_{sfc}(x,y) = \varepsilon_0(x,y)^{-1/4}T^B(x,y), \quad (10)$$

where $\varepsilon_0(x,y)$ is surface emissivity, it can be derived from vegetation coverage P_v (Valor and Caselles 1996), i.e.

$$\varepsilon_0(x,y) = \varepsilon_v(x,y)P_v(x,y) + \varepsilon_g(x,y)(1-P_v(x,y)) + 4\langle\varepsilon\rangle(1-P_v(x,y))P_v(x,y), \quad (11)$$

where $\varepsilon_v(x,y)$ and $\varepsilon_g(x,y)$, are surface emissivity for full vegetation and bare soil respectively, $\langle\varepsilon\rangle$ is the error item.

3.2 *Soil heat flux density*

The regional soil heat flux density $G_0(x,y)$ is determined through (Choudhury and Monteith 1988)

$$G_0(x,y) = \rho_s C_s \frac{[T_{sfc}(x,y) - T_s(x,y)]}{r_{sh}(x,y)}, \quad (12)$$

where ρ_s is soil dry bulk density, C_s is soil specific heat, $T_s(x,y)$ represents soil temperature of a determined depth, and $r_{sh}(x,y)$ stands for resistance of soil heat transportation. The regional soil heat flux density $G_0(x,y)$ cannot directly be mapped from satellite observations through Eq. (12). Many investigations have shown that the mid-day G_0/R_n ratio, Γ, is reasonably predictable from special vegetation indices (Daughtry et al. 1990). Γ can be considered as a function F which relates G_0/R_n to other variables (Ma 2001). Some researchers have concluded that $G_0/R_n = \Gamma = F(NDVI)$ (Clothier et al. 1986; Kustas and Daughtry 1990). A better ratio of $G_0/R_n = \Gamma = F(r_0, T_{sfc}, NDVI)$ was also found (Choudhury et al. 1987; Menenti et al. 1991; Bastiaanssen 1995). A parameterization scheme based on the MSAVI has been found over the HEIFE area as

$$G_0(x,y) = R_n(x,y)\cdot[T_{sfc}(x,y)/r_0(x,y)] \cdot (0.00028 + 0.004364\bar{r}_0 + 0.00846\bar{r}_0^2) \cdot [1 - 0.97892MSAVI(x,y)^4], \quad (13)$$

where $\bar{r}_0$ is surface reflectance averaged over the period when the soil is heated from the sun. Surface temperature T_{sfc} is expressed in degrees Celsius. $MSAVI(x,y)$ is derived from the band reflectance of the Landsat TM as (Qi et al. 1994).

$$MSAVI(x,y) = \left(2r_4(x,y) + 1 - \sqrt{[2r_4(x,y)+1]^2 - 8[r_4(x,y) - r_3(x,y)]}\right)/2, \quad (14)$$

where r_3 and r_4 are the band reflectance of the Landsat TM Band-3, and Band-4 on the land surface.

3.3 *Sensible heat flux density*

The regional distribution of sensible heat flux density is calculated from

$$H(x,y) = \rho C_p \frac{T_{sfc}(x,y) - T_a(x,y)}{r_a(x,y)}, \quad (15)$$

where aerodynamic resistance is

$$r_a(x,y) = \frac{1}{ku_*(x,y)}\left[\ln\left(\frac{z-d_0(x,y)}{Z_{0m}(x,y)}\right) + kB^{-1}(x,y) - \psi_h(x,y)\right], \quad (16)$$

where k is Von-Karman constant; u_* friction velocity; z reference height; d_0 zero-plane displacement height; Z_{0m} the effective aerodynamic roughness; kB^{-1} excess resistance for heat transportation; and, ψ_h the stability correction function for heat. The friction velocity u_* can be derived from

$$u(x,y) = \frac{u_*(x,y)}{k}\left[\ln\left(\frac{z-d_0(x,y)}{Z_{0m}(x,y)}\right) - \psi_m(x,y)\right], \quad (17)$$

where ψ_m is the stability correction function for momentum.

From Eqs. (15), (16) and (17),

$$H(x,y) = \rho C_p k^2 u(x,y)(T_{sfc}(x,y) - T_a(x,y))/ ([\ln(z-d_0(x,y))/(Z_{0m}(x,y)) + kB^{-1}(x,y) - \psi_h(x,y)] \cdot [\ln(z-d_0(x,y))/(Z_{0m}(x,y)) - \psi_m(x,y)]). \quad (18)$$

One approach to simulate sensible heat flux density on a large scale is to scale-up, or aggregate the regional sensible flux by a weighted average of the contributions from different surface elements, based on the principle of flux conservation. A method of "blending height" is proposed to derive the regional sensible heat flux density in this study. If the local-scale advection is comparatively small during the period of the Landsat TM observation taking place, the development of convection boundary layer may adjust the surface-disorganized variability at "blending height", where the atmospheric characteristics become proximately independent of the horizontal position. The corresponding 'effective' surface variables can be determined accordingly (Mason 1988). This approach has been proved to be successful to calculate areally averaged surface fluxes in recent years (Lhomme et al. 1994; Bastiaassen 1995; Wang et al. 1995; Ma et al. 1999). Based on this approach, the regional sensible heat flux density $H(x,y)$ can be described as

$$H(x,y) = \rho C_p k^2 u_B(T_{sfc}(x,y) - T_a(x,y))/ ([\ln(z_B - d_0(x,y))/(Z_{0m}(x,y)) + kB^{-1}(x,y) - \psi_h(x,y)] \cdot [\ln(z_B - d_0(x,y))/(Z_{0m}(x,y)) - \psi_m(x,y)]), \quad (19)$$

where z_B is blending height and u_B is the wind speed at the blending height. In this study, z_B and u_B are determined with the aid of field measurements of tethersonde and sodar. $Z_{0m}(x,y)$ is the effective aerodynamic roughness length including the effect of topography and vegetation (e.g. crop field). It is calculated by using Taylor's model (Taylor et al. 1989). kB^{-1} is the excess resistance, which can be determined from the leaf area index (LAI) by using a widely-used model (Qualls and Brutsaert 1995). d_0 is zero-plane displacement, which can be calculated from the leaf area index (LAI) by using Raupach's model (Raupach 1994).

$T_a(x,y)$ in Eq. (19) is the regional distribution of air temperature at the reference height. Air temperature was estimated from satellite thermal infrared data by Davies and Tarpley (1983), Bastiaanssen (1995), Wang et al. (1995) and Ma et al. (1999). It was found that there is a positive correlation between T_a and the surface radiative temperature T_{sfc}. A better numerical interpolation method to derive the distribution of air temperature from remotely sensed surface temperature, was used to analyze the "urban heat island effect" (Wu et al. 1993; Ding 1989). An improved interpolation method is proposed here to derive the regional distribution of air temperature over the oasis-desert system. The remotely sensed surface temperature is taken as the initial temperature field, and it is smoothed by the smoothing method of nine points

$$T^*_{sfc(i,j)} = [4T_{sfc(i,j)} + 2(T_{sfc(i+1,j)} + T_{sfc(i-1,j)} + T_{sfc(i,j+1)} + T_{sfc(i,j-1)}) + T_{sfc(i+1,j+1)} + T_{sfc(i-1,j+1)} + T_{sfc(i+1,j-1)} + T_{sfc(i-1,j-1)}]/16. \quad (20)$$

It indicates that the smoothing value of surface temperature $T^*_{0(i,j)}$ on the point (i,j) can be obtained. If there are a number of observation

sites, the difference between the smoothing surface temperature $T^*_{sfc(k)}$ and the observation air temperature $T_{a(k)}$ can be derived from

$$dT_{a(k)} = T^*_{sfc(k)} - T_{a(k)}. \quad (21)$$

If the difference between the smoothing surface temperature, and the air temperature on grid point (i, j) is $DT_a(i, j)$ and $dT_1, dT_2, \ldots, dT_m$ are the differences between the smoothing surface temperature, and the observation air temperature on No. 1, No. 2,..., No. m observation sites, $DT_a(i, j)$ can be written as

$$DT_a(i, j) = \Sigma[dT_{a(k)}/r_k^2]/\Sigma r_k^{-2} \quad (k = 1, 2 \ldots m), \quad (22)$$

where r_k is the distance between the observation point k and the grid point (i, j). The difference $dT_{a(k)}$ on the observation point can be interpolated to all the grid points (i, j) from Eq. (22). Air temperature on each grid point (i, j) can be derived as

$$T_a(i, j) = T_{sfc}(i, j) - DT_a(i, j). \quad (23)$$

In other words, the regional distribution of air temperature $T_a(x, y)$ can be derived using this improved numerical interpolation method based on a number of field observations of air temperature, and regional surface temperature.

$\psi_h(x, y)$ and $\psi_m(x, y)$ in Eq. (19) are the integrated stability functions. For unstable condition, the integrated stability functions $\psi_h(x, y)$ and $\psi_m(x, y)$ can be written as (Paulson 1970)

$$\begin{cases} \psi_m(x, y) = 2\ln[(1+X)/2] + \ln[(1+X^2)/2] \\ \qquad\qquad - 2\arctan(X) + 0.5\pi \\ \psi_h(x, y) = 2\ln[(1+X^2)/2] \end{cases} \quad (24)$$

where $X = \{1 - 16[z - d_0(x, y)]/L(x, y)\}^{0.25}$. For stable condition, the integrated stability function $\psi_m(x, y)$ and $\psi_h(x, y)$ become (Webb 1970)

$$\psi_m(x, y) = \psi_h(x, y) = -5[z - d_0(x, y)]/L(x, y). \quad (25)$$

The stability function $[z - d_0(x, y)]/L(x, y)$ is calculated by Businger's method (Businger 1988).

$$\begin{cases} [z - d_0(x, y)]/L(x, y) = R_i(x, y) \quad (unstable) \\ [z - d_0(x, y)]/L(x, y) \\ \qquad = R_i(x, y)/[1 - 5.2R_i(x, y)] \quad (stable) \end{cases}, \quad (26)$$

where $R_i(x, y)$ is the Richardson number.

3.4 *Latent heat flux density*

The regional latent heat flux density $\lambda E(x, y)$ can be derived as the residual of the energy budget theorem for land surface based on the condition of zero horizontal advection at $z < z_{sur}$ (this is not always true in the HEIFE area, Wang et al. 1993), i.e.

$$\lambda E(x, y) = R_n(x, y) - H(x, y) - G_0(x, y). \quad (27)$$

4. Case study and validation

Figure 3 shows the distribution maps of surface reflectance, vegetation coverage, LAI, MSAVI, NDVI and land surface heat flux densities over the HEIFE area based on 2600 × 2600 pixels with a size of about 28.5 × 28.5 m^2. The distribution map of surface temperature in Fig. 3 is based on 2600 × 2600 pixels with a size of about 120 × 120 m^2. The frequency distributions of land surface variables, vegetation variables and land surface flux densities are shown in Fig. 4. The derived land surface variables, and land surface heat flux densities, can be validated by field measurements. In Fig. 5 the derived results are plotted against the measured values in the field for the surface reflectance, surface temperature and four terms of the energy balance. The 1:1 line is also plotted in the graphs. The surface reflectance and surface temperature, which were obtained from the regression relationship, and land surface heat flux densities derived from the SEBAL (Wang et al. 1995; Ma et al. 1999) are plotted in Fig. 5 as well. The differences between the old methods (Wang et al. 1995; Ma et al. 1999) and this research are shown in Table 1. Since it is difficult to determine where the exact locations of the experimental sites are, the values of a 5 × 5 pixel rectangle, surrounding the determined Universal Transfer Macerator (UTM) coordinate, are compared with the field measurements. The mean absolute percent difference (MAPD) can quantitatively measure the difference between the derived results ($H_{derived(i)}$) and measured values ($H_{measured(i)}$) as

$$MAPD = \frac{100}{n}\sum_{i=1}^{n}\left(\frac{|H_{derived(i)} - H_{measured(i)}|}{H_{measured(i)}}\right). \quad (28)$$

The derived, and measured land surface variables, (surface reflectance and surface tempera-

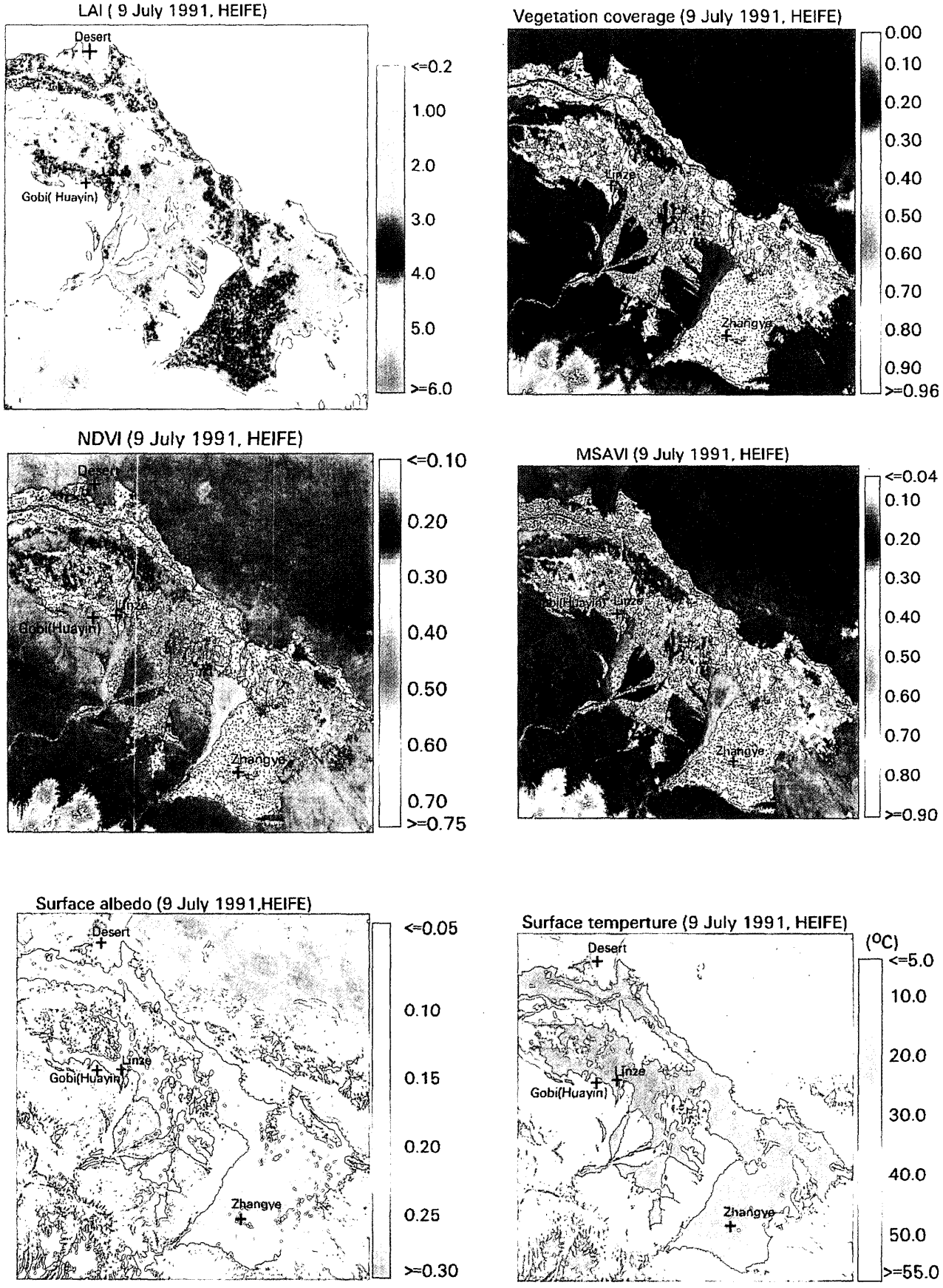

(a)

Fig. 3. Maps of land surface variables, vegetation variables and land surface heat flux densities for the HEIFE area. 10:00 (LST), July 9, 1991. (a) land surface variables and vegetation variables and (b) land surface heat flux densities.

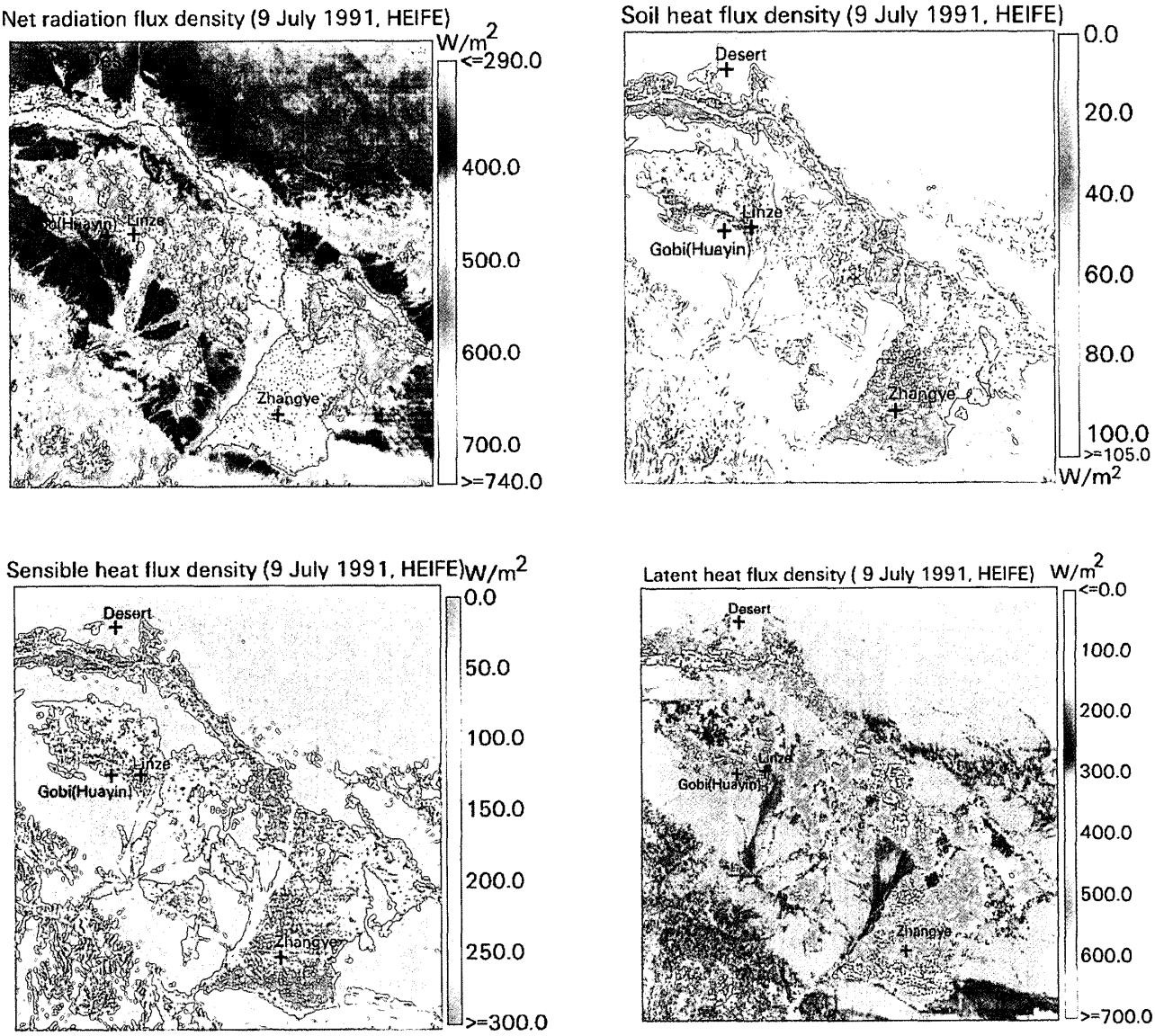

(b)

Fig. 3 (continued)

ture) and land surface heat flux densities in different stations are shown in Table 2. Their MAPD are also shown in Table 2.

It can be seen that: (1) the derived land surface variables, vegetation variables and heat flux densities over the HEIFE area are in good accordance with the land surface status (Fig. 1). These parameters show a wide range due to the strong contrast of surface features and there are two peaks in the figures of all frequency distributions in this area. The first peak corresponds to the oasis, and another one corresponds to the Gobi desert (see Table 3); (2) the derived NDVI with atmospheric correction is more reasonable than the previous results derived by Wang et al. (1995) and Ma et al. (1999). The distribution ranges of the NDVI in oasis, and Gobi desert become wider than previous results, and its distribution peak in oasis become much more clear. The previous results (Wang et al. 1995; Ma et al. 1999) are not good, due to atmospheric correction in their procedure of calculating the NDVI; (3) the derived surface reflectance and surface temperature in this research is better than the results derived from the linear regression relationship (Wang et al. 1995; Ma et al. 1999), and the MAPD is less than 10%. There are some shortages exist-

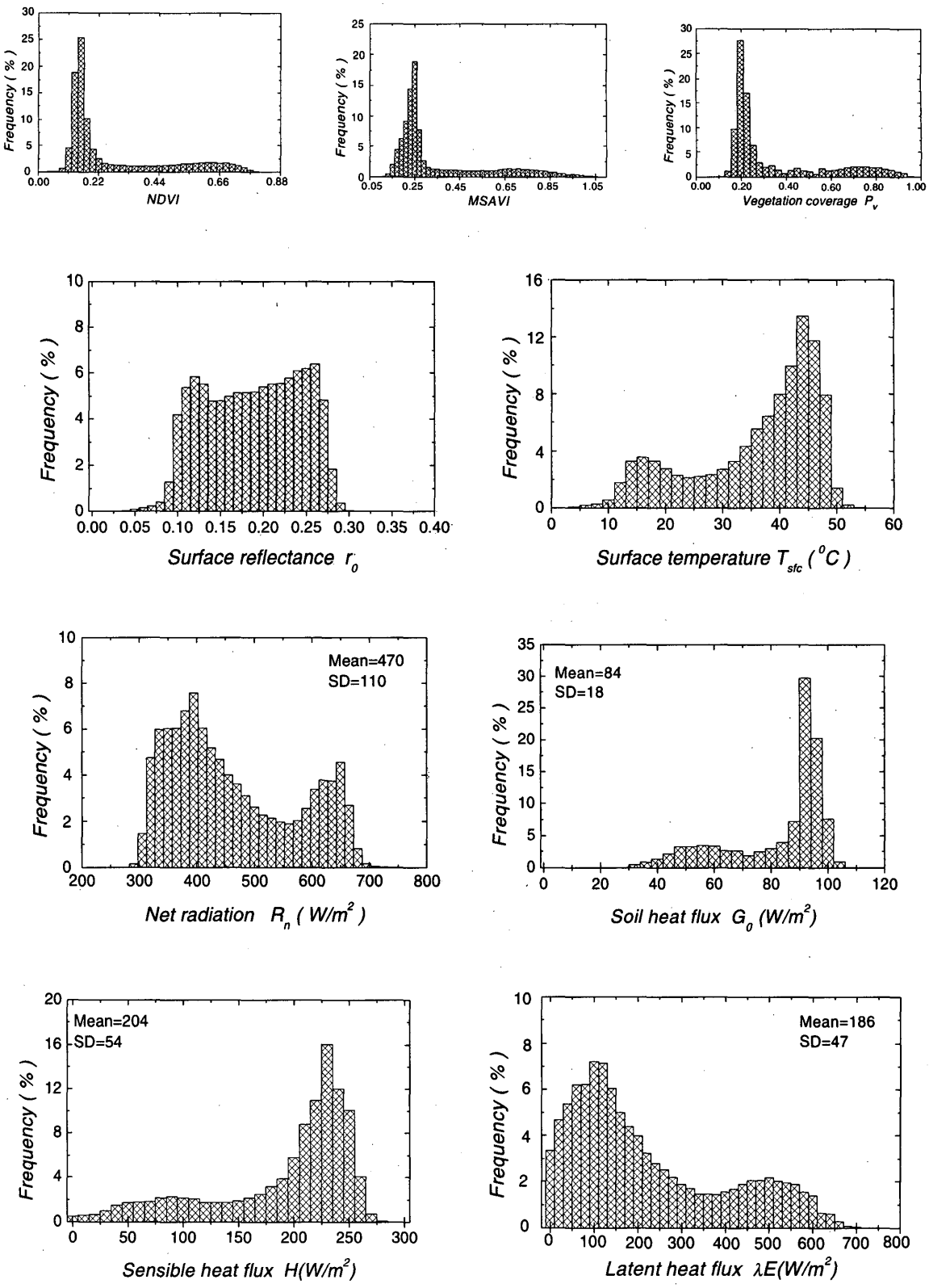

Fig. 4. Frequency distribution of land surface variables, vegetation variables and land surface heat flux densities for the HEIFE area. 10:00 (LST), July 9, 1991.

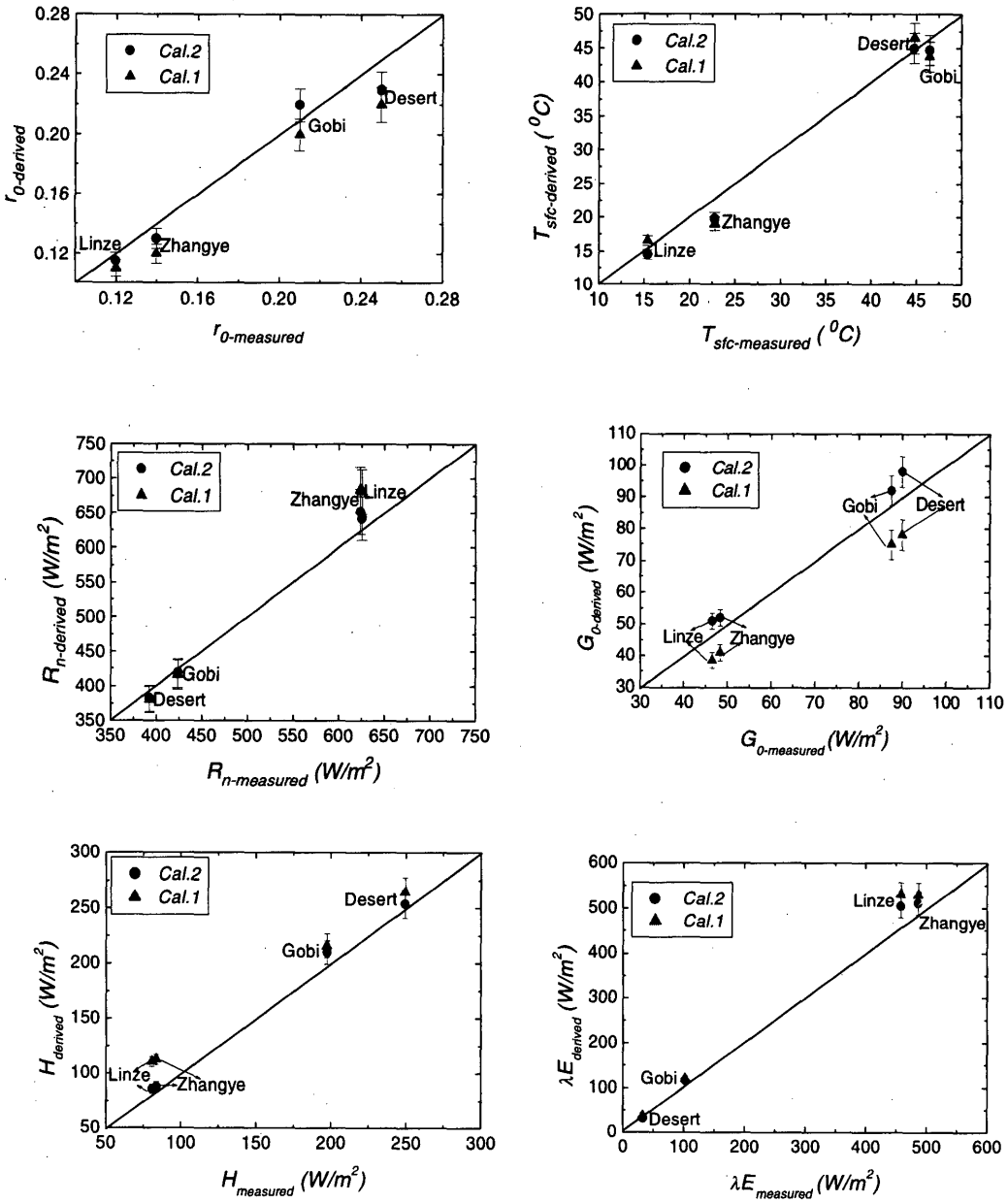

Fig. 5. Validation of the derived results against the field measurements for the surface reflectance, surface temperature and land surface heat flux densities over the HEIFE area, together with 1:1 line. Cal. 2: derived results in this paper; Cal. 1: results by Wang et al. (1995) and Ma et al. (1999).

ing in the procedure of deriving surface reflectance and surface temperature from the linear regression relationship, i.e.: a) the ground measurement is only a point value, while the satellite pixel is the average of many point values; b) fewer ground observation data are coincidence with satellite data, when the satellite overpasses the observation sites, therefore more sophisticated measurement techniques are needed; and, c) geo-resignation should be accurately made in the establishment of the regression relationship. Hence, surface reflectance and surface temperature derived from the four-stream radiative transfer assumption for atmospheric correction are better than it derived from the linear regression relationship due to its better considering in the radiative transfer process and overcoming the shortages. It means that the four-stream radiative transfer assumption for atmospheric correction, which used to derive surface reflectance, and the retrieval method for regional surface tem-

Table 1. The comparison of parameterization procedure between the previous methods (Wang et al. 1995; Ma et al. 1999) and this method.

	Algorithms	
Items	This method	Previous methods
$r_0(x,y)$	four –stream transfer assumption	1)linear regression between r_0 and r_p
$T_{sfc}(x,y)$	radiative transfer equation (4)	2)linear regression between $L_0\uparrow$ and L_{TOA}
$NDVI(x,y)$	$NDVI=f(r_3, r_4)$ with atmospheric correction	$NDVI=f(r_3, r_4)$ without atmospheric correction
$MSAVI(x,y)$	equation (13)	no
$P_v(x,y)$	3)$P_v=[\frac{NDVI-NDVI_{min}}{NDVI_{max}-NDVI_{min}}]^2$ (Carlson and Ripley 1997)	no
$LAI(x,y)$	4)$LAI=-\frac{1}{2k}\ln[\frac{r_0-r_v}{r_s-r_v}]$ (Ma, 2001)	no
$\varepsilon_0(x,y)$	$\varepsilon_0=f(P_v)$	$\varepsilon_0=f(NDVI)$
$K_\downarrow(x,y)$	MODTRAN model	5)$K_\downarrow(x,y)=\overline{K_\downarrow}=\frac{1}{n}\sum_{i=1}^{n}K_{\downarrow_i}$
$L_\downarrow(x,y)$	MODTRAN model	6)$L_\downarrow(x,y)=\overline{L_\downarrow}=\frac{1}{n}\sum_{i=1}^{n}L_{\downarrow_i}$
$G_0(x,y)$	equation (12)	$G_0=f(NDVI)$
$H(x,y)$ $T_a(x,y)$	derived from surface temperature T_{sfc} by numerical interpolation method	linear regression between air temperature T_a and surface temperature T_{sfc}
$kB^{-1}(x,y)$	$kB^{-1}=f(LAI)$	2.3
$Z_{0m}(x,y)$	Taylor's model	$Z_{0m}=f(NDVI)$
$d_0(x,y)$	$d_0=f(LAI)$	7)$d_0=\frac{2}{3}h$

1)r_p : planetary reflectance;

2) L_{TOA} : the thermal infrared band radiance at the top of atmosphere measured by TM; $L_0\uparrow$: upward long wave radiation measured in the stations;

3) $NDVI_{min}$ and $NDVI_{max}$: $NDVI$ values for bare soil and full vegetation respectively;

4) r_s and r_v: surface reflectance for bare soil and full vegetation;

5) $\overline{K_\downarrow}$: mean downward short wave radiation, $K_{\downarrow_i}$: downward short wave radiation observed in the station No.i;

6) $\overline{L_\downarrow}$: mean downward long wave radiation, $L_{\downarrow_i}$: downward long wave radiation observed in the station No.i;

7) h: canopy height.

perature in this research can be used over heterogeneous landscape; (4) the derived net radiation is very close to the field measurement with the MAPD less than 5%. It is better than the former results (Wang et al. 1995; Ma et al. 1999) due to the improvements in $r_0(x,y)$, $T_{sfc}(x,y)$, $\varepsilon_0(x,y)$, $K_\downarrow(x,y)$ and $L_\downarrow(x,y)$; (5) problems exist in the NDVI definition equation because of the external factor effect, such as soil back-ground variations (Huete et al. 1985; Huete 1989). To reduce the soil back-ground effect, Qi et al. (1994) proposed using the MSAVI. Therefore, the parameterization method based on the MSAVI for soil heat flux density is better than it based on the NDVI on heterogeneous land surface. Although the derived regional soil

Table 2. The mean absolute percent difference (MAPD) between the derived results (Cal. 1 and Cal. 2) and measured (Meas.) values at the HEIFE site. Cal. 2: derived results in this paper; Cal. 1: results by Wang et al. (1995) and Ma et al. (1999)

	r_0 (-)					T_{sfc} (°C)				
	Meas.	*Cal. 2*	*MAPD*	*Cal. 1*	*MAPD*	*Meas.*	*Cal. 2*	*MAPD*	*Cal. 1*	*MAPD*
Desert	0.25	0.23	8.00%	0.22	12.01%	44.8	45.0	0.45%	46.5	3.79%
Linze	0.12	0.11	8.30%	0.11	8.30%	15.4	14.5	5.84%	16.5	7.14%
Gobi	0.21	0.22	4.76%	0.20	4.76%	46.5	44.7	3.87%	43.7	6.02%
Zhangye	0.14	0.13	7.14%	0.12	14.28%	22.8	20.7	9.21%	19.0	16.76%
	R_n (W m^{-2})					G_0 (W m^{-2})				
	Meas	*Cal. 2*	*MAPD*	*Cal. 1*	*MAPD*	*Meas.*	*Cal. 2*	*MAPD*	*Cal. 1*	*MAPD*
Desert	392.6	382.0	2.71%	380.5	3.08%	90.0	98.0	8.89%	78.0	13.33%
Linze	625.7	640.0	2.28%	680.5	8.76%	46.5	51.0	9.67%	38.5	17.11%
Gobi	423.6	418.0	1.32%	416.0	1.79%	87.5	92.0	5.14%	75.0	14.20%
Zhangye	623.7	652.0	4.54%	683.5	9.59%	48.3	52.0	7.66%	41.0	15.13%
	H (W m^{-2})					λE (W m^{-2})				
	Meas.	*Cal. 2*	*MAPD*	*Cal. 1*	*MAPD*	*Meas.*	*Cal. 2*	*MAPD*	*Cal. 1*	*MAPD*
Desert	249.5	254.0	1.80%	265.0	6.21%	33.0	30.0	9.10%	37.5	13.64%
Linze	80.8	86.0	6.43%	110.5	36.76%	458.0	503.0	9.80%	531.5	16.05%
Gobi	197.5	210.0	6.33%	216.0	9.37%	108.5	116.0	6.91%	120.5	11.06%
Zhangye	83.7	88.0	5.14%	112.5	34.42%	486.5	512.0	5.19%	530.5	9.04%

Table 3. The distribution range and peaks of land surface variables, vegetation variables and land surface heat flux densities over the HEIFE area.

	range	oasis (peak)	Gobi desert (peak)
NDVI	0.10—0.75	~0.66	~0.15
MSAVI	0.08—0.92	~0.80	~0.25
P_v	0.00—0.95	~0.78	~0.20
r_0	0.04—0.30	~0.12	~0.26
LAI	0.00—5.80	~2.80	~0.45
T_{sfc} (°C)	5.0—55.0	~16.0	~44.0
R_n (W/m^2)	290—750	~650	~380
G_0 (W/m^2)	30—105	~50	~90
H (W/m^2)	0—300	~90	~230
λE (W/m^2)	0—700	~500	~100

heat flux based on the MSAVI is a bit higher than the measured value, the MAPD gets smaller than the former derived value based on the NDVI (Wang et al. 1995; Ma et al. 1999); (6) the green-yellow parts in the distribution map of sensible heat flux, except the mountainous area in the southwest (lower-left), are mainly oasis areas consisting of crop field, small woods and wet soil, with a relatively low value of sensible heat flux between 0 W/m^2 and 120 W/m^2. The red-violet-blue areas, which form most of the map, are mainly drier sand desert and Gobi with much higher sensible heat flux between 140 W/m^2 and 300 W/m^2. The derived regional sensible heat flux densities with the MAPD of around 5% at four validation sites are in good accordance with the field measurements. The peaks of oasis and Gobi desert in the histogram of sensible heat flux distribution (Fig. 4.) are clearer than the previous results (Wang et al. 1995; Ma et al. 1999). The derived sensible heat flux by using improvement method is much better than the previous results (Wang et al. 1995; Ma et al. 1999) due to the improvement in calculating the scheme of regional air temperature $T_a(x, y)$, $kB^{-1}(x, y)$,

$Z_{0m}(x, y)$ and $d_0(x, y)$. The previous results derived from SEBAL could be used over the Gobi and sand desert surface (MAPD = 9.37% and MAPD = 6.21%), but there is a large difference between the derived results and the field-measured values over oasis (MAPD = 36.76% in Linze and MAPD = 34.40% in Zhangye); and (7) the derived regional latent heat flux density, which is based on the energy balance equation, is acceptable for the whole HEIFE area. The value calculated from MAPD is less than 10% for the four validation sites.

5. Concluding remarks

In this study, the regional distributions of land surface variables (surface reflectance and surface temperature), vegetation variables (the NDVI, the MSAVI and vegetation coverage) and land surface heat flux densities (net radiation, soil heat flux, sensible and latent heat flux), over heterogeneous area of the HEIFE are derived with the aid of the Landsat TM data and the field observation. Compared with previous studies (Wang et al. 1995; Ma et al. 1999) the new method has proved to be a better approach to getting related air-land parameters over heterogeneous landscape due to the improvements in old parameterizations (Wang et al. 1995; Ma et al. 1999). This study forms a sound basis to study land surface variables, vegetation variables and land surface flux densities.

Dealing with the regional land surface heat flux densities over heterogeneous landscape is not an easy problem. The parameterization method presented in this research is still in the developing stage: 1) From Eq. (17), it is better to use air temperature, and wind speed at the reference height when we calculate the sensible heat flux. But we only propose one method to calculate regional air temperature at reference height in this research, therefore the "blending height" approach has to be used. The wind speed at the reference height over the HEIFE area should be derived by using some numerical models, and the spatial resolution of the models should be 28.5 m × 28.5 m; 2) Only a single set of values at a specific time of specific day are used in this research. To reach more accurate regional land surface flux densities, more field observations and another satellite such as NOAA (National Oceanic and Atmospheric Administration)/AVHRR (Advanced Very High Resolution Radiometer), GMS (Geostationary Meteorological Satellite) and ATSR (Along Track Scanning Radiometer) have to be used. These research works will be done in the next step.

The vegetation variables cannot be validated in this research due to no such measurements during the HEIFE experiment. It should be paid more attention on the measurements of vegetation variable, such as NDVI, LAI and vegetation coverage, in the future experiment.

Acknowledgements

This work was under the auspices of the Chinese National Key Programme for Developing Basic Sciences (G1998040900), the Innovation Project of Chinese Academy of Sciences (KZCX2-301) and the Innovation Project of Cold and Arid Regions Environmental and Engineering Research Institute, Chinese Academy of Science (CACX210072 and CACX210039). Some parts of this study were done as cooperative research works in the Disaster Prevention Research Institute, Kyoto University and the Alterra Green World Research, Wageningen UR, the Netherlands. The authors acknowledge Profs. M. Maitani, E. Ohtaki, K. Sahashi, T. Koike and Dr. K. Ueno for their kind help and useful discussions. We are grateful to the referees for their very useful comments and helpful suggestions, which contributed to the final version of the manuscript.

References

Bastiaanssen, W.G.M., 1995: Rigionalization of surface flux densities and moisture indicators in composite terrain. *PhD thesis, Wageningen Agricultural University*, Wageningen, the Netherlands, 143–161.

Berk, A., L.S. Bernstein, and D.C. Robertson, MODTRAN, 1989: A moderate resolution model for LOTRAN 7. GL-TR-89-0122.

Businger, J.A., 1988: A note on the Businger-Dyer profiles. *Bound. Layer Meteor.*, **42**, 145–151.

Carlson, T.N. and Ripley, D.A., 1997: On the relation between NDVI, fractional vegetation cover, and leaf area index. *Remote Sens. Environ.*, **62**, 241–252.

Chodhury, B.J., Idso, S.B., and Reginato, R.J., 1987: Analysis of an empirical model for soil heat flux under a growing wheat crop for estimating

evaporation by infrared-temperature based energy balance equation, *Agricultural and Forest Meteorology*, **39**, 283–297.

——— and J.L. Monteith, 1988: A four-layer model for the heat budget of homogeneous land surfaces. *Quart. J. Roy. Meteor. Soc.*, **114**, 373–398.

Clothier, B.E., K.L. Clawson, P.J. Pinter, M.S. Moran, R.J. Reginato, and R.D. Jackson, 1986: Estimating of soil heat flux from net radiation during the growth of alfalfa. *Agricultural and Forest Meteorology*, **37**, 319–329.

Daughtry, C.S.T., Kustas, W.P., Moran, M.S., Pinter, P.J., Jackson, R.D., Brown, P.W., Nichols, W.D., and Gay, L.W., 1990: Spctral estimates of net radiation and soil heat flux. *Remote Sens. Environ.*, **32**, 111–124.

Davis, P.A. and J.D. Tarpley, 1983: Estimation of shelter temperature from operational satellite sounder data, *J. Climate Appl. Meteor.*, **22**, 369–376.

Ding, Y., 1989: The diagnostic analysis methodology in the dynamic weather, Science Press, Beijing, pp. 13 (in Chinese).

Hu, Y., Gao, Y., Wang, J., Ji, G., Shen, Zh., Cheng, L., Chen, J., and Li, Sh., 1994: Some achievements in scientific research during HEIFE. *Plateau Meteorology*, **13**, 225–236. (in Chinese with English abstract).

Huete, A.R., Jackson, R.D., and Post, D.F., 1985: Spectral response of a plant canopy with different soil backgrounds. *Remote Sens. Environ.*, **17**, 37–53.

———, 1989, Soil influences in remotely sensed vegetation-canopy spectra. *Theory and Applications of Optical Remote Sensing* (G. Asrar, Ed.), 107–141.

Kenizys, F.X., Abreu, L.W., Anderson, G.P., Chetwynd, J.H., Shettle, E.P., Berk, A., Bernstein, L.S., Robertson, D.c., Acharya, P., Rothman, L.S., Selby, J.E.A., Gallery, W.O., and Clough, S.A., 1996: *The MODTRAN3/2 report and LODTRAN 7 Model.* (L.W. Abreu and G.P. Andson, Eds) Prepared by Ontar Corp., North Andover, MA, for Phillips Laboratory, Geophysical Directorate, Hanscom AFB, MA., Contract No. F19628-91-C-0132.

Koepke, P., K.T. Kriebel, and B. Dietrich, 1985: The effect of surface reflection and of atmospheric parameters on the short wave radiation budget. *Advances in Space Research*, **5**, 353–354.

Kustas, W.P. and C.S.T. Daughtry, 1990: Estimation of the soil heat flux/net radiation ratio from spectral data. *Agricultural and Forest Meteorology*, **39**, 205–223.

Lhomme, J.-P., A. Chehbouni, and B. Monteny, 1994: Effective parameters of surface energy balance in heterogeneous landscape. *Bound. Layer Meteor.*, **71**, 297–310.

Ma, Y., Wang, J., Menenti, M., and Bastiaanssen, 1999: Estimation of flux densities over the heterogeneous land surface with the aid of satellite remote sensing and field observation. *ACTA Meteor. Sinica*, **57**, 180–189 (in Chinese with English abstract).

———, 2001: Parameterization of land surface heat flux densities over inhomogeneous landscape by combining satellite remote sensing with field observations, *PhD thesis, Okayama University*, Japan, 1–195.

Maitani, T., Sahashi, K., Ohtaki, E., Tsukamoto, O., Mitsuta, Y., and Wang, J., 1995: Measurements of turbulent fluxes and model simulation of micrometeorology in a wheat field at Zhangye oasis. *J. Meteor. Soc. Japan*, **73**, 959–965.

Mason, P., 1988: The formation of areally averaged roughness lengths. *Quart. J. Roy. Meteor. Soc.*, **114**, 399–420.

Menenti, M., Bastiaanssen, W.G.M., and D. Van Eick, 1989: Determination of hemispheric reflectance with Thematic Mapper data. *Remote Sens. Environ.* (special issue), **28**, 327–337.

———, Bastiaanssen, W.G.M., Hefny, K., and Abd EI Karim, M.H., 1991: Mapping of ground water losses by evaporation in the Western Desert of Egypt. *DLO Winand Staring Centre, Report no. 43*, Wageningen, The Netherlands, 1–116.

Mitsuta, Y., Tamagawa, I., Sahashi, K., and Wang, J., 1995: Estimation of annual evaporation from the Linze desert during HEIFE. *J. Meteor. Soc. Japan*, **73**, 967–974.

Paulson, C.A., 1970: The mathematic representation of wind speed and temperature profiles in the unstable atmospheric surface layer. *J. Appl. Meteor.*, **9**, 856–861.

Qi, J., A. Chehbouni, A.R. Huete, Y.H. Kerr, S. Sorooshian, 1994: A Modified Soil Adjusted Vegetation Index. *Remote Sens. Environ.*, **48**, 119–126.

Qualls, R.J. and W. Brutsaert, 1995: The effect of vegetation density on the parameterization of scalar roughness to estimate spatially distributed sensible heat fluxes. *Water Resources Research*, **32**, 645–652.

Raupach, M.R., 1994: Simplified expressions for vegetation roughness length and zero-plane displacements as functions of canopy height and area index. *Bound. Layer Meteor.*, **71**, 211–216.

Sahashi, K., 1995: A wet period in the desert station in HEIFE. *J. Meteor. Soc. Japan*, **73**, 1213–1217.

Taylor, P.A., R.I. Sykes, and P.J. Mason, 1989: On the parameterization of drag over small scale

topography in neutrally stratified Boundary flow. *Bound. Layer Meteor.*, **48**, 409–422.

Tamagawa, I., 1996: Turbulent characteristics and bulk transfer coefficients over the desert in the HEIFE area. *Bound. Layer Meteor.*, **77**, 1–20.

Tsukamoto, O., Wang, J., and Mitsuta, Y., 1992: A significant Evening peak of vapour pressure at an oasis in the semi-arid region. *J. Meteor. Soc. Japan*, **70**, 1155–1159.

———, Sahashi, K., and Wang, J., 1995: Heat budget and evapotranspiration at an oasis surface surrounded by desert. *J. Meteor. Soc. Japan*, **73**, 925–935.

Valor, E. and V. Caselles, 1996: Mapping land surface emissivity from NDVI: Application to European, African and South American Area. *Remote Sens. Environ.*, **57**, 167–184.

Verhoef, W., 1997: Theory of radiative transfer models applied in optical remote sensing of vegetation canopies. *PhD thesis, Remote Sensing Department of National Aerospace Laboratory*, The Netherlands.

Wang, J., K. Sahashi, E. Ohtaki, T. Maitani, O. Tsukamoto, Y. Mistsuta, T. Kobayashi, H. Zhang, Q. Li, and Z. Xie, 1993: Energy and mass transfer characteristics of soil-vegetation-atmosphere system in oasis area-Outline of the bio meteorological observation period (BOP). *Proceedings of International Symposium on HEIFE*, Nov. 8–11, 1993, Kyoto, 507–514.

——— and Y. Mitsuta, 1990: Peculiar downward water vapor flux over Gobi desert in the daytime. *J. Meteor. Soc. Japan*, **68**, 399–402.

——— and Y. Mitsuta, 1992: An observation study of turbulent study of turbulent structure and transfer characteristics in Heihe oasis. *J. Meteor. Soc. Japan*, **70**, 1147–1154.

———, Ma, Y., Menenti, M., W. Bastiaanssen, and Y. Mistsuta, 1995: The scaling-up of processes in the heterogeneous landscape of HEIFE with the aid of satellite remote sensing. *J. Meteor. Soc. Japan*, **73**, 1235–1244.

Webb, E.K., 1970: Profile relationships: the log-liner range and extension to strong stability, *Quart. J. Roy. Meteor. Soc.*, **96**, 67–90.

Wen, J., 1999: Land surface variables estimated from remote sensing and the correction of atmospheric effects. *Ph.D. Thesis, Lanzhou Institute of Plateau Atmospheric Physics, The Chinese Academy of Sciences*, Lanzhou, China, 1–115 (in Chinese with English abstract).

Wu, K., Wang, X., Wang, Sh., Zhao, W., Yang, F., and Pan, Zh., 1993: An analysis of urban island effect for air temperature using NOAA satellite data. *ACTA Meteor. Sinica*, **51**, 203–208 (in Chinese with English abstract).